Design of Cyclodextrin/Aptamer-Based Dual Recognition Fluorescent Sensor for Sensitive Detection of Galectin-3

Phoomintara Longsompurana, Nongluk Plongthongkum, Tassaneewan Laksanasopin, and Rungtiva P. Poo-arporn*

Biological Engineering Program, Faculty of Engineering, King Mongkut's University of Technology Thonburi, Thailand
Email: chemistrymvk@gmail.com (P. L.); nongluk.plo@kmutt.ac.th (N. P.); tassaneewan.lak@kmutt.ac.th (T. L.); rungtiva.pal@kmutt.ac.th (R. P.P.)
*Corresponding author

Manuscript received November 20, 2024; accepted February 14, 2025; published June 13, 2025

***Abstract*—Early detection of Heart Failure (HF) is crucial for enhancing patient outcomes, and recent developments in non-invasive biomarker sensors have enabled monitoring at the early stages to achieve this goal. In this study, we developed an HF detection platform targeting the biomarker Galectin-3 (Gal3), utilizing two specific binding sites: β hexakis-(6-mercapto-6-deoxy)-β-cyclodextrin (mCD) and an aptamer binding site. Computational methods, such as molecular docking, were employed to select and design an aptamer with enhanced binding affinity for Gal3. The engineered aptamer, Apt4_C15A, demonstrated strong binding affinity to Gal3, as confirmed through fluorescence assays, with a low equilibrium dissociation constant (K_D) of 3.20 ± 1.25 μM. The sensor was constructed as a sandwich platform, with mCD functionalized on silver-coated plates serving as the primary capture molecule and a 6-carboxyfluorescein amidite (FAM)-tagged aptamer serving as both the secondary capture molecule and fluorescent signal probe. The sensor exhibited high sensitivity, achieving a detection limit of 11.03 ng/mL within a linear range of 10–200 ng/mL, effectively covering clinically relevant Gal3 concentrations. This innovative mCD/aptamer-based fluorescent sensor demonstrated excellent detection performance, underscoring its potential as a reliable platform for early HF biomarker detection. Future improvements will focus on optimizing sensor fabrication conditions to minimize non-specific binding, further enhancing sensor accuracy and robustness.**

***Keywords*—aptamer, cyclodextrin, fluorescent sensor, Galectin-3, heart failure, molecular docking**

I. Introduction

Heart Failure (HF) is a prevalent and critical health condition that requires early detection to improve patient outcomes. However, traditional diagnostic methods often fail to identify HF in its early stages. Emerging biomarker sensors represent a promising advancement, enabling non-invasive monitoring for early HF detection and ongoing health assessment. The integration of advanced biosensors into HF detection strategies has the potential to improve clinical outcomes by supporting timely diagnoses, individualized treatment approaches, and proactive disease management, thereby reducing hospital admissions and healthcare costs [1]. Among these, fluorescent sensors integrated with aptamers (Apts) offer advantages. Aptamers, known for their high specificity, stability, and strong affinity for a wide range of targets, significantly enhance the selectivity and sensitivity of fluorescent sensors, enabling the precise detection of low concentrations of HF biomarkers at early stages [2, 3]. Additionally, aptamers can be synthesized and modified with ease, making them a cost-effective and versatile alternative to antibodies. The post-systematic evolution of ligands by exponential enrichment (post-SELEX) method enhances aptamer binding affinity by iteratively selecting high-affinity sequences, thereby improving the performance of aptamer-functionalized sensors. Furthermore, molecular simulation and docking techniques play a crucial role in optimizing aptamer design. These computational methods predict aptamer-target interactions and identify high-affinity binding sites, enabling the rational design of aptamers with improved specificity and affinity [4].

In recent years, significant advancements have been made in developing Gal3 sensors leveraging the interaction between saccharides and Gal3, achieving high sensitivity [3, 5, 6]. Building on this progress, this study proposes the integration of beta-cyclodextrin (βCD), a cyclic oligosaccharide with unique properties, to enable specific host-guest interactions for enhanced Gal3 detection [7].

This study proposes the design of a novel fluorescent-based Gal3 sensor using a dual recognition platform. The platform integrates mCD as the primary specific binding molecule and a fluorescent-tagged aptamer that functions as the secondary specific binding molecule and fluorescent probe. Additionally, we selected a new Gal3 aptamer and designed it using molecular simulation and molecular docking. We hypothesize that the sensor could achieve a clinically relevant detection range, with potential applications in HF biomarker detection.

II. Methodology

A. Gal3-mCD Interactions

To create the detection platform, the sensor was designed based on the structure of the target protein, Gal3, with two designated binding sites (Fig. 1a). The first binding site on Gal3 was assigned as the Hexakis-(6-mercapto-6-deoxy)-β-cyclodextrin (mCD) binding site, while the second was designated as the aptamer binding site.

The mCD binding site was identified on the Gal3 structure (Fig. 1a) through molecular docking between mCD and Gal3. The mCD structure was prepared by substituting the oxygen atoms of the primary hydroxyl groups in the β-cyclodextrin (βCD) structure from Protein Data Bank (PDB) (PDB ID: 1Z0N) with sulfur atoms to form thiol groups. It was optimized using the Gaussian (G09) program with the theoretical basis set HF/6-31G [8] before performing molecular docking with Gal3 (PDB ID: 3ZSJ) utilizing a global docking technique with the AutoDock Vina program

(version 1.1.2) [9].

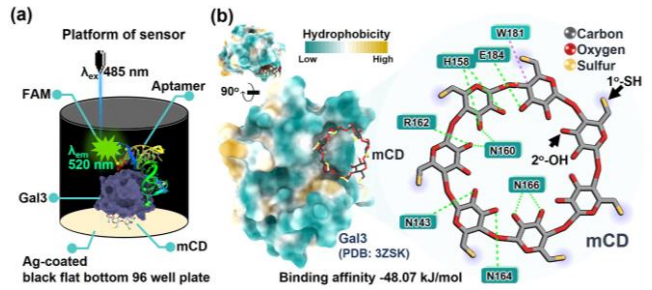

Fig. 1. (a) Platform of the Gal3 fluorescent sensor. (b) Interaction between Gal3 and mCD, evaluated through molecular docking using AutoDock Vina, interactions were analyzed by BIOVIA Discovery Studio Visualizer.

B. Development of Gal3 Aptamer

To select the Gal3 aptamer candidates, the 3D structures of 20 aptamers obtained from PDB were prepared by removing heteroatoms and molecules before Gal3-aptamer docking. We identified lead Gal3 aptamers that bind to the aptamer binding site (at residues 125–133: A, 135–137: A, 169: A, 187–193: A, 195–229: A, and 241–250: A) without overlapping with the mCD binding site. The 3D structures of the aptamers and Gal3 were then uploaded to the HDOCK server (http://hdock.phys. hust.edu.cn/) [10] to predict binding site. Subsequently, the torsions of the unfavorable bonding residues were optimized using the AMBER (ff14sb) force field before rescoring with AutoDock Vina to determine the binding affinity values (kJ/mol) [11]. Aptamers that exhibited the highest binding affinity were identified as lead aptamers and designed using site-directed mutagenesis to modify a specific base. The designed aptamer underwent energy minimization before being docked with Gal3, followed by rescoring with AutoDock Vina to calculate its binding affinity.

C. Determination of Equilibrium Dissociation Constant

The Gal3 concentration of 1 µg/mL in 0.01 M PBS pH 7.4 was incubated in a black flat-bottom 96-well plate overnight. The unbound Gal3 was removed by PBS. The 6-carboxyfluorescein amidite (FAM)-tagged aptamer (0.015–8 µM) in Tris-HCl buffer containing 0.5 M sodium chloride (NaCl), 10 mM Tris-HCl, and 1 mM magnesium chloride ($MgCl_2$) at pH 7.4 was incubated for 2 hours, and the unbound Gal3 was removed by Tris-HCl buffer. PBS pH 12.0 was added to activate the chromophore of FAM for 10 minutes before fluorescent measurements at an excitation wavelength (λ_{ex}) of 485 nm and an emission wavelength (λ_{em}) of 520 nm. Finally, the equilibrium dissociation constant (K_D) was calculated by fitting the data using (1) [12].

$$\mathrm{F(520\ nm)} = \frac{\mathrm{F}_{max} \times [\mathrm{Apt}]}{K_D + [Apt]} \quad (1)$$

where F is fluorescence intensity at λ_{ex} 485 nm and λ_{em} 520 nm; [Apt], the concentration of the aptamer candidates (µM); F_{max}, the maximum fluorescence intensity and K_D, equilibrium dissociation constant (µM).

D. Design of Gal3 Fluorescent Sensor

To prepare the mCD/silver (Ag)-coated black flat-bottom 96-well plate, Tollen's reagent was freshly prepared according to the method reported by Chen *et al.* [13] and 100 µL was dispensed into each well of the plate. Immediately afterward, 100 µL of a 100 mM glucose solution was added to each well and incubated for three minutes, resulting in the Ag-coated plate. The plate was then rinsed several times with DI water to remove excess reactants and allowed to dry. Next, 40 µL of 1 mM mCD (in DMSO) was added to each well of the Ag-coated plate and incubated for two hours to form a silver-thiol bond, resulting in the mCD/Ag-coated plate. Afterward, 100 µL of 10–200 ng/mL Gal3 in 0.01 M PBS, pH 7.4 was added and incubated overnight to immobilize it on the mCD/Ag-coated plate. Unbound Gal3 was removed by rinsing with PBS (pH 7.4). Subsequently, 50 nM FAM-labeled aptamer in Tris-HCl buffer (pH 7.4) was added and incubated at 4 °C for two hours. Unbound aptamers were removed by rinsing with Tris-HCl buffer. To activate the FAM fluorophore of the bound FAM-labeled aptamer, 100 µL of PBS (pH 12.0) was incubated for 10 minutes. Fluorescence intensity was measured with excitation at a wavelength (λ_{ex}) of 485 nm and emission (λ_{em}) at 520 nm. The fluorescent signal from Gal3 on mCD/Ag was assigned as F, and the signal from the FAM-labeled aptamer in the absence of Gal3 on mCD/Ag was assigned as F_0, setting the background signal. Thus, the actual signal for Gal3 detection is represented by ΔF, which was calculated using Eq. (2).

$$\Delta F = F - F_0 \quad (2)$$

where ΔF is different fluorescence intensity, F is the fluorescence intensity of aptamer on Gal3/mCD/Ag, and F_0 is the fluorescent intensity of aptamer on mCD/Ag.

III. Results and Discussions

A. Interaction of mCD/Gal3

The structure of Gal3 was docked with mCD to identify mCD binding site within the Gal3 structure. The result in Fig. 1b reveal a perfect fit between Gal3 and the mCD structure. The docking output of mCD/Gal3 confirms the ability of mCD to bind to the hydrophilic groove, a component of the Carbohydrate-Recognition Domain (CRD) of Gal3, with a binding affinity of −48.07 kJ/mol. This observation suggests that the hydroxyl groups in mCD play a crucial role in Gal3 binding, as the structure fits almost perfectly into Gal3's hydrophilic groove. This interaction is mediated primarily through hydrogen bonding with polar-rich amino acids, including glutamine (Q) 143, 160, 164, and 166; histidine (H) 158; arginine (R) 162; and glutamate (E) 184, as well as a hydrophobic interaction with tryptophan (W) 181.

B. Development of Gal3 Aptamer

To identify potential lead aptamers with specific binding to Gal3, we analyzed a dataset containing 20 DNA aptamers. The selection of lead aptamers was based on their interaction with the aptamer binding site on Gal3 and their ability to promote the highest binding affinity. As anticipated, Apt4_1TOB (see Fig. 2) facilitated binding to the aptamer binding site on Gal3, with the highest binding affinity of −73.85 kJ/mol.

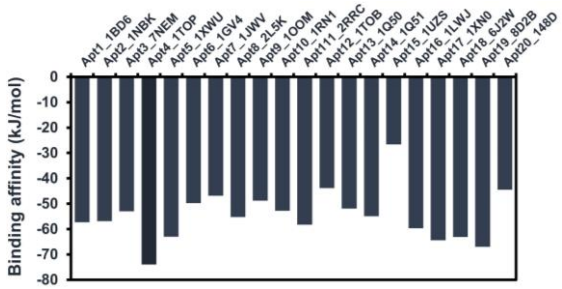

Fig. 2. Selection of the lead aptamer for Gal3 through molecular docking using the HDOCK server, with binding affinity evaluated by rescoring through AutoDock Vina.

Fig. 3a demonstrates that the Cytosine (C) at position 15 of Apt4_1TOB was mutated to Adenine (A), resulting in Apt4_C15A. Fig. 3b shows the modified sequence, validated by its two-Dimensional (2D) secondary structure, represented in dot-bracket notation through RNAfold (http://rna.tbi.univie.ac.at/) [14], which confirmed that the 2D structure of Apt4_C15A was identical to the original Apt4_1TOB, with a calculated folding free energy of −76.95 kJ/mol. To confirm the improved binding affinity, Apt4_C15A was redocked with Gal3 structures (PDB IDs: 3ZSJ, 3ZSK, 6RZH, 6I74, 6QLR) and compared to Apt4_1TOB. Fig. 3c demonstrates that Apt4_C15A exhibited a higher average binding affinity (−76.29±2.24 kJ/mol), indicating a stronger binding interaction with Gal3 than the Apt4_1TOB aptamer (−74.04±3.76 kJ/mol). We suggest that Apt4_C15A was a reliable aptamer for the further development of Gal3 fluorescent sensors. This study also suggests that Thymine (T) and Guanine (G) at this position should be mutated to investigate their effects on binding affinity.

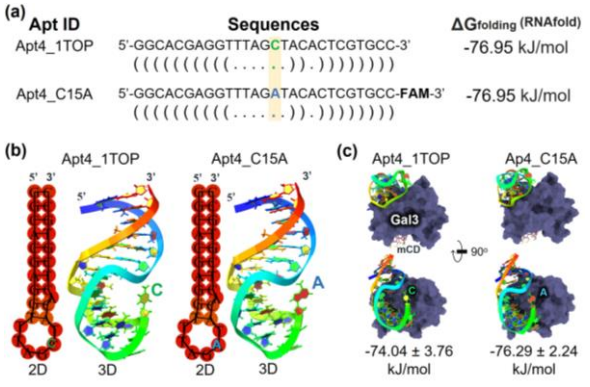

Fig. 3. Molecular simulation and calculation: (a) dot-bracket notation and predicted folding energy of aptamers, (b) 2D and 3D structures of aptamers, and (c) binding posture and binding affinity of aptamers with Gal3 predicted through HDOCK sever, binding affinities calculated by AutoDock Vina.

To characterize the properties of fluorescence, the Apt4_C15A was synthesized with a 3'-FAM tag (named Apt4_C15A-FAM) by Integrated DNA Technologies (IDT) Pte. Ltd. (Singapore). The Apt4_C15A-FAM was characterized by UV-Vis and fluorescence spectroscopy using a Tecan Infinite M200 fluorescence microplate reader (Männedorf, Switzerland). Fig. 4 demonstrates that Apt4_C15A-FAM exhibits a characteristic peak in the UV-Vis absorption spectrum at 260 nm [15], representing the absorption of nitrogenous bases in the DNA aptamer, as well as the absorption characteristic of FAM at 495 nm [16]. Meanwhile, the FAM fluorophore exhibits a excitation wavelength (λ_{ex}) at 495 nm and an emission wavelength (λ_{em}) at 520 nm [17], generating bright green fluorescence (Fig. 4 inset).

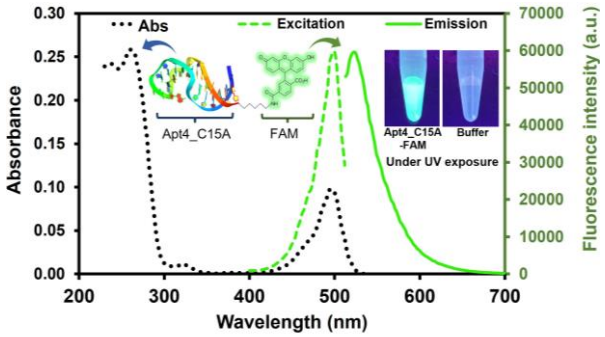

Fig. 4. The optical properties of Apt4_C15A-FAM (3 µM) in PBS buffer at pH 12.0: (black dots) UV-Vis absorbance, (green dashed line) excitation, and (green solid line) emission spectra at pH 12.0.

To maximize the fluorescence intensity of the sensor and reduce noise background, the optimum detection parameters were investigated. Fig. 5a shows that Apt4_C15A-FAM in PBS buffer at pH 12.0 demonstrated the highest fold change in fluorescence intensity with a lag time of 5 µs and an integration time of 40 µs at an excitation wavelength of 485 nm. The choice of lag time can significantly impact fluorescence measurements, particularly in fluorescence techniques. An optimal lag time helps eliminate background fluorescence and scatter from short-lived, non-specific signals. Since the FAM fluorophore decays rapidly, a lag time longer than 5 µs could cause its signal to be undetectable by the time the measurement begins. Meanwhile, longer integration times at the optimal lag time increase the amount of collected fluorescence signal, improving the signal-to-noise ratio (S/N ratio). This was especially beneficial for detecting weak or low-abundance signals, enhancing sensitivity at low target concentrations. These findings indicate that these optimal conditions produce higher intensity compared to the blank (PBS pH 12.0) solution and help reduce background signal from PBS. Although FAM has a maximum excitation wavelength of 495 nm, it was not suitable for sensing due to limitations of the device, which has fixed broad excitation (9 nm) and emission (20 nm) spectra, resulting in overlapping excitation and emission spectra. This phenomenon can cause unwanted emissions from the excitation light itself, leading to a high intensity signal from the blank and a low S/N ratio (low fold change in fluorescence intensity). This study demonstrated that using an excitation wavelength of 485 nm significantly reduced the background fluorescence signal from the blank, resulting in a greater fold change in fluorescence intensity.

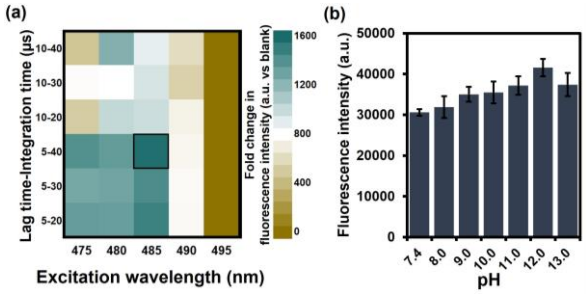

Fig. 5. Optimization of (a) detection parameters of the fluorescence spectroscopy in PBS buffer at pH 12.0 at λ_{em} 520 nm, and (b) detection pH measured at λ_{ex} 485 nm and λ_{em} 520 nm (1 µM Apt4_C15A-FAM in black flat-bottom 96-well plate), (N = 3, mean ± SD).

In addition, the pH of the detection solution is a crucial factor for fluorophore activation. Fig. 5b demonstrates that Apt4_C15A-FAM exhibited the highest fluorescence intensity at pH 12.0. Under more basic conditions, the carboxyl group of FAM becomes deprotonated, leading to a more conjugated and stable electronic state. This deprotonated state enhances fluorescence by allowing greater resonance and stabilization in the excited state, producing strong bright green fluorescence [18].

Following the engineering of the Apt4_C15A-FAM aptamer, its binding affinities were investigated using the fluorescent assay. Fig. 6 depicts the binding affinity, represented by the equilibrium dissociation constant (K_D) values. Notably, the Apt4_C15A-FAM aptamer exhibits a low K_D value of 3.20±1.25 μM, indicating a high binding affinity to the Gal3 protein.

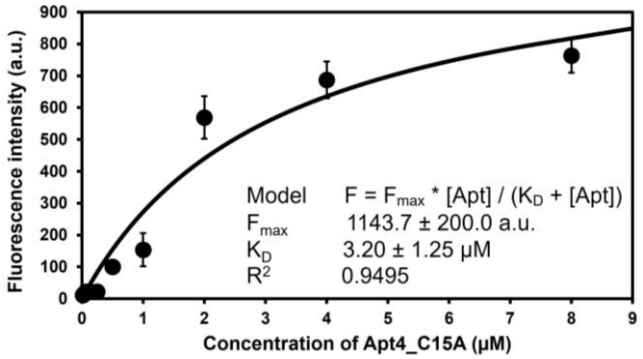

Fig. 6. The equilibrium dissociation constant (KD) for the binding between Apt4_C15A-FAM (0.015–8 μM) and Gal3 (1 μM) was measured at λ_{ex} 485 nm and λ_{em} 520 nm in PBS buffer at pH 12.0 (N = 3, mean ± SD).

To validate the designed sandwich fluorescence sensor, the mCD/Ag-coated plate was prepared (see inset in Fig. 7). Apt4_C15A-FAM-FAM was incubated with mCD/Ag-coated plates and mCD/Ag-coated plates with Gal3 (1 μg/mL), and their fluorescence intensity was measured at pH 12.0. Fig. 7 demonstrates that Apt4_C15A-FAM interacts significantly with Gal3 on the mCD/Ag-coated plate compared to mCD/Ag-coated plates alone and the blank (buffer on the mCD/Ag-coated plate). This finding confirms that the sandwich fluorescent sensor was suitable for Gal3 sensing. However, we suggest that an appropriate washing buffer and optimal concentration of aptamer should be further investigated to reduce non-specific binding of the aptamer on the mCD/Ag plate.

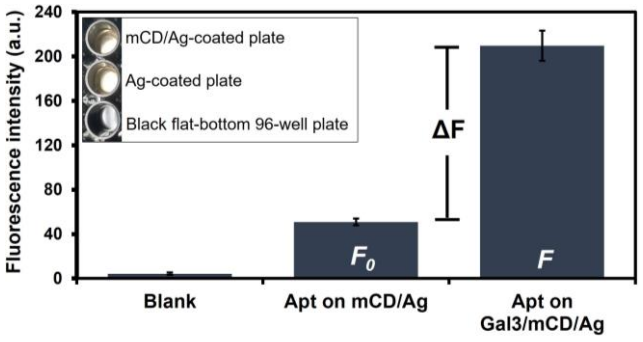

Fig. 7. Evaluation of the interaction between Apt4_C15A-FAM (50 nM) and different modified plates. All experiments were measured at λ_{ex} 485 nm and λ_{em} 520 nm in PBS buffer at pH 12.0. (N = 3, mean ± SD).

C. Detection Performance of Gal3 Fluorescent Sensor

In order to investigate the attributes of the mCD with aptamer as a sandwich sensor for a fluorescence-based Gal3 sensor, the dynamic detection linear range was firstly determined. Fig. 8 depicts the fluorescent signal responses of the sensor: as the concentration of Gal3 increases, the ΔF signal also increases. It becomes evident that the sensor exhibited linear behavior within the concentration range of 10 to 200 ng/mL, with the linear regression equation as follows: $\Delta F = 0.7967[\text{Gal3}] + 0.0532$. The data fitting is remarkably accurate, as indicated by the high confidence coefficient of $R^2 = 0.9577$. The sensor demonstrated a Limit of Detection (LOD) of 11.03 ng/mL (S/N = 3) and a limit of quantification (LOQ) of 36.75 ng/mL (S/N = 10). Consequently, the system demonstrates the ability to accurately detect Gal3 concentrations within the clinically relevant cut-off level of 17.8 ng/mL. However, we also recommend investigating additional aspects of the sensor's performance, including selectivity and real sample tests, to further enhance its reliability and efficacy.

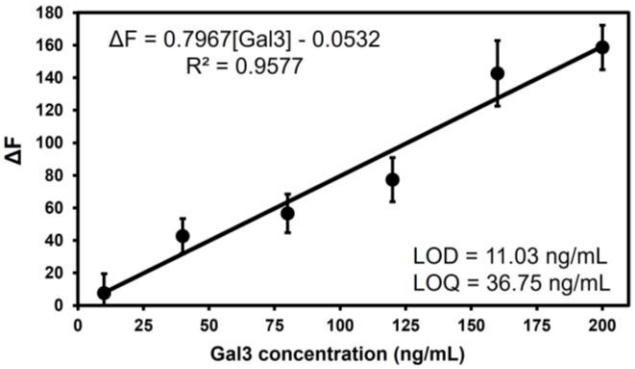

Fig. 8. Calibration curve for the determination of Gal3 (10–200 ng/mL) with Apt4_C15A-FAM (50 nM), measured at λ_{ex} 485 nm and λ_{em} 520 nm in PBS buffer at pH 12.0. (N = 3, mean ± SD).

IV. Conclusions

This study describes the design and development of a highly specific Galectin-3 (Gal3) fluorescent sensor utilizing a cyclodextrin/aptamer-based dual recognition technique. Molecular docking confirmed that mCD specifically binds to Gal3's hydrophilic groove, which is crucial for its high binding affinity. Molecular simulations and docking were effective in designing and enhancing the aptamer's binding affinity, with a low equilibrium dissociation constant (K_D) indicating a strong interaction with Gal3. As expected, the cyclodextrin/aptamer sandwich fluorescent sensor proved effective, exhibiting a broad linear range within clinically relevant detection limits. This sensor design holds promise for early and accurate Gal3 detection, supporting potential applications in diagnostic assays. Further refinements, including screening additional aptamer libraries, optimizing fabrication procedures, and evaluating sensor performance, could further enhance its efficacy.

Conflict of Interest

The authors declare no conflict of interest.

Author Contributions

P. L. conducted the investigation, methodology, data curation, visualization, and writing—original draft. N. P.

conducted the methodology. T. L. conducted the methodology. R. P. P. conducted the conceptualization, methodology, funding acquisition, writing—review & editing, and supervision. All authors had approved the final version.

FUNDING

This research project is supported by King Mongkut's University of Technology Thonburi (KMUTT), Thailand Science Research and Innovation (TSRI), and National Science, Research and Innovation Fund (NSRF) Fiscal year 2025 Grant number (FRB680074/0164) P. L. would like to thank the Petchra Pra Jom Klao Ph.D. Research Scholarship for financial support.

REFERENCES

[1] S. I. Kaya, A. Cetinkaya, G. Ozcelikay, S. N. Samanci, and S. A. Ozkan, "Approaches and challenges for biosensors for acute and chronic heart failure," *Biosensors*, vol. 13, no. 2, p. 282, Feb 2023.

[2] W. Zhang, J. Jiang, T. Liu, X. Wang, Y. Wang, Z. Chu, and W. Jin, "A rapid and ultrasensitive cardiac troponin I aptasensor based on an ion-sensitive field-effect transistor with extended gate," *Talanta*, 126364, Sep 2024.

[3] Z. Zhang, Y. Yu, Y. Zhao, and K. M. Ng, "A fluorescent nanoparticle probe based on sugar-substituted tetraphenylethene for label-free detection of galectin-3," *J. Mater. Chem. B*, vol. 7, no. 43, pp. 6737–6741, Oct 2019.

[4] Q.-L. Wang, H.-F. Cui, J.-F. Du, Q.-Y. Lv, and X. Song, "In silico post-SELEX screening and experimental characterizations for acquisition of high affinity DNA aptamers against carcinoembryonic antigen," *RSC Adv.*, vol. 9, no. 11, pp. 6328–6334, Feb 2019.

[5] Y. K. Park, B. Bold, W. K. Lee, M. H. Jeon, K. H. An, S. Y. Jeong, and Y. K. Shim, "D-(+)-galactose-conjugated single-walled carbon nanotubes as new chemical probes for electrochemical biosensors for the cancer marker galectin-3," *Int. J. Mol. Sci.*, vol. 12, no. 5, pp. 2946–2957, May 2011.

[6] M. C. Martos-Maldonado, I. Quesada-Soriano, L. García-Fuentes, and A. Vargas-Berenguel, "Multivalent lactose–ferrocene conjugates based on poly (amido amine) dendrimers and gold nanoparticles as electrochemical probes for sensing Galectin-3," *Nanomater.*, vol. 10, no. 2, p. 203, Jan 2020.

[7] S. Saffarionpour and L. L. Diosady, "Preparation and characterization of an iron–β-cyclodextrin inclusion complex: Factors influencing the host–guest interaction," *Food & Function*, vol. 14, no. 11, pp. 5062–5077, May 2023.

[8] O. Guendouzi, A. Guendouzi, H. B. Ouici, H. Brahim, M. Boumediene, and M. Elkeurti, "A quantum chemical study of encapsulation and stabilization of gallic acid in β-cyclodextrin as a drug delivery system," *Canadian Journal of Chemistry*, vol. 98, no. 4, pp. 204–214, Mar 2020.

[9] O. Trott and A. J. Olson, "AutoDock Vina: Improving the speed and accuracy of docking with a new scoring function, efficient optimization, and multithreading," *J. Comput. Chem.*, vol. 31, no. 2, pp. 455–461, Jan 30, Jan 2010.

[10] Y. Yan, D. Zhang, P. Zhou, B. Li, and S. Y. Huang, "HDOCK: A web server for protein-protein and protein-DNA/RNA docking based on a hybrid strategy," *Nucleic. Acids. Res.*, vol. 45, no. W1, pp. W365–W373, Jul 2017.

[11] A. O. Zalevsky, A. S. Zlobin, V. R. Gedzun, R. V. Reshetnikov, M. L. Lovat, A. V. Malyshev, I. I. Doronin, G. A. Babkin, and A. V. Golovin, "PeptoGrid—Rescoring function for AutoDock Vina to identify new bioactive molecules from short peptide libraries," *Mol.*, vol. 24, no. 2, p. 277, Jan 2019.

[12] F. T. C. Moreira, S. Sharma, R. A. F. Dutra, J. P. C. Noronha, A. E. G. Cass, and M. G. F. Sales, "Protein-responsive polymers for point-of-care detection of cardiac biomarker," *Sens. Actuators B: Chem.*, vol. 196, pp. 123–132, Jun 2014.

[13] Z. Chen, X. Chen, L. Zheng, T. Gang, T. Cui, K. Zhang, and B. Yang, "A simple and controlled method of preparing uniform Ag midnanoparticles on Tollens-soaked silica spheres," *J. Colloid. Interface Sci.*, vol. 285, no. 1, pp. 146–151, May 2005.

[14] I. L. Hofacker, "Vienna RNA secondary structure server," *Nucleic. Acids. Res.*, vol. 31, no. 13, pp. 3429–3431, Jul 2003.

[15] W. Zhang, M. Luo, J. Chen, Z. Li, X. Wei, M. Wu, S. Yang, Y. He, X. Wang, and Z. Xiao, "A simple and label-free fluorescent DNA sensor for visual detection of aptamer-based berberine," *Analytical Methods*, vol. 42, no. 16, pp. 7130–7138, Sep 2024.

[16] M. Marieeswaran and P. Panneerselvam, "Fluorescent polyaniline nanoclips (PANCs): A highly sensitive and selective chemical sensor for the detection of Hg (II) ions in aqueous media," *Chemistry Select*, vol. 5, no. 15, pp. 4481–4487, Apr 2020.

[17] Y. Wu, X. Chen, X. Wang, M. Yang, F. Xu, C. Hou, and D. Huo, "A fluorescent biosensor based on prismatic hollow Metal-polydopamine frameworks and 6-carboxyfluorescein (FAM)-labeled protein aptamer for CA15-3 detection," *Sens. Actuators B: Chem.*, vol. 329, 129249, Feb 2021.

[18] F. Le Guern, V. Mussard, A. Gaucher, M. Rottman, and D. Prim, "Fluorescein derivatives as fluorescent probes for pH monitoring along recent biological applications," *Int. J. Mol. Sci.*, vol. 21, no. 23, p. 9217, Dec 2020.